

Full length article

Transcutaneous tumor vaccination combined with anti-programmed death-1 monoclonal antibody treatment produces a synergistic antitumor effect

Xinran Song^{a,1}, Yuxin Jiang^{b,1}, Weixing Zhang^c, Gomaa Elfawal^{a,d}, Kaili Wang^a, Di Jiang^a, Huoyan Hong^a, Jinglei Wu^a, Chuanglong He^a, Xiumei Mo^a, Hongsheng Wang^{a,*}

^a Shanghai Engineering Research Center of Nano-Biomaterials and Regenerative Medicine, Key Laboratory of Science & Technology of Eco-Textile, Ministry of Education, College of Chemistry, Chemical Engineering and Biotechnology, Donghua University, Shanghai 201620, PR China

^b Department of Pathogenic Biology and Immunology, School of Medicine, Jiaxing University, Jiaxing, 314001, PR China

^c Department of Critical Care Medicine, Shanghai General Hospital, Shanghai Jiao Tong University, School of Medicine, Shanghai 201600, PR China

^d Polymer Materials Department, Advanced Technology and New Materials Research Institute, Scientific Research and Technological Applications City (SRTA-City), New Borg El-Arab City, Alexandria, 21934, Egypt

ARTICLE INFO

Article history:

Received 26 February 2021

Revised 20 November 2021

Accepted 23 November 2021

Available online 27 November 2021

Keywords:

Transcutaneous immunization

Dendritic cells

Anti-programmed death-1 monoclonal antibody

Ethosome

Antitumor

ABSTRACT

Transcutaneous immunization (TCI) has the advantages of safety, high efficiency, non-invasiveness and convenient use. The key for a TCI system is transdermal targeted delivery of antigen to dendritic cells (DCs), the most powerful antigen presenting cells. DCs also play an important role in tumor immunotherapy, which provides a huge imagination for the application of TCI to tumor treatment. In this study, a transcutaneous tumor vaccine (TTV) delivery system was developed using the electrospun silk fibroin (SF) and polyvinyl alcohol (PVA) composite nanofibrous patch loaded with mannosylated polyethyleneimine (PEI^{man})-modified ethosome (Eth) (termed Eth-PEI^{man}). Eth-PEI^{man} showed a good performance in targeting DCs, and the carriers loaded with antigen (encapsulated in Eths) and adjuvant (adsorbed in PEI^{man}) were observed effectively induce DCs maturation in vitro. With the tyrosinase-related protein-2 (TRP2) peptide as antigen and oligodeoxynucleotides containing unmethylated CpG motifs as adjuvant, the TTV-loaded patches (TTVP) significantly inhibited the growth of melanoma in a syngeneic mouse model for melanoma by subcutaneous injection of B16F10 cell lines. Moreover, the combined application of the TTVP and anti-programmed death-1 monoclonal antibody (aPD-1) produced a synergistic antitumor effect, which could be related to the infiltration of more CD4⁺ and CD8⁺ T cells in the tumor tissues. The application of TTVP also increased the expression of IL-12, which may be part of the mechanism of synergistic antitumor effect between the TTVP and aPD-1. These results suggest that the combination of the TTVP and immune checkpoint blockers could be an effective strategy for tumor treatment.

Statement of significance

Transcutaneous immunization has the advantages of safety, high efficiency, non-invasiveness and convenient use. In this study, a novel transcutaneous tumor vaccine patch (TTVP) was developed using tumor antigens-loaded ethosomes that can target dendritic cells percutaneously. Our data demonstrated that the TTVP can significantly inhibit tumor growth. Furthermore, the combination of TTVP and aPD-1 produced a synergistic anti-melanoma effect. Considering its convenience and non-invasiveness, this TTVP system could find good application prospects in immunotherapy. The combination of TTVP and aPD-1 could be a useful strategy for the prevention and treatment of tumors.

© 2021 Acta Materialia Inc. Published by Elsevier Ltd. All rights reserved.

1. Introduction

Dendritic cells (DCs) are the professional and most powerful antigen presenting cells (APCs), which stimulate initial and acquired immune responses by internalizing and processing anti-

* Corresponding author.

E-mail address: whs@dhu.edu.cn (H. Wang).

¹ Authors contributed equally

gens and presenting them to T cells [1,2]. The active epidermal and dermal layers of skin tissue are rich in DCs, which makes the skin one of the best sites for immunization and give birth to the concept of transcutaneous immunization (TCI) [3,4]. TCI is a new method of vaccination, in which the antigen and adjuvant are topically applied to the intact skin surface to induce an immune response. Compared with traditional subcutaneous or intramuscular vaccination methods, TCI has the following advantages [4–6]: good safety (avoiding potential infections caused by acupuncture wounds or needle contamination), good compliance (eliminating children's fear of needle vaccination), high efficiency (a small amount of antigen can trigger an effective immune response) and easy to use (no special medical workers are needed and thus the cost is greatly saved).

The success of TCI depends on making the macromolecular antigen molecules break through the stratum corneum and target DCs. Ethosome (Eth) is a special liposome containing a certain concentration of alcohol (20%–45%), which have a smaller particle size, higher encapsulation efficiency and better flexibility [7]. Eth has been demonstrated to be an useful carrier for transdermal drug delivery [8–12]. Our recent research showed that Eths can effectively carry biomacromolecules into skin tissues and induce specific immune responses [13]. There are C-type lectin receptors on the surface of DCs, including mannose receptor, DEC-205 and DC-Sign, etc. [14]. Antigen-loaded carriers decorated by mannose have been proved to be able to target DCs and effectively trigger immune response [15,16]. Therefore, Eths modified with materials containing mannose groups can be useful for TCI.

In addition to specific antigens (usually peptides with 8–10 amino acids), the effective activation of DCs and related CTL activities often requires the combined application of adjuvants to stimulate powerful immune response [17]. Oligodeoxynucleotides containing unmethylated CpG motifs (CpGs) is considered to be one of the most effective adjuvants and have attracted much attention in immunotherapy [18,19]. These CpGs are common in the bacterial or viral genome, but are suppressed and methylated in the vertebrate genome [20]. CpGs can be captured by the cell surface receptor DEC-205 and delivered to the intracellular Toll-like receptor 9 (TLR9), which stimulates B cells, macrophages and DCs to secrete Th1-like cytokines (such as IL-12, IL-18, and co-stimulatory molecules (CD80 and CD86), etc.) inducing a strong Th1 response and enhancing antigen presentation [21–23]. However, the applications of CpGs is limited because they are easily degraded and has low internalization efficiency [24,25]. Hence, it is essential to protect CpGs from degradation and increase its delivery efficiency in immunotherapy. Polyethyleneimine (PEI) has been used as a promising non-viral vector for gene delivery because of its high efficiency of transfection, low immunogenicity and easy production [26,27]. PEI plays a vital role on protecting DNA from nuclease degradation by concentrating DNA to form compact nanoscale complexes [27–29]. The good performance of PEI for protection and delivery of CpGs has been confirmed recently [29]. Moreover, the mannosylated PEI (PEI^{man}) showed a good ability to target DCs [30–32]. Therefore, we hypothesize that the PEI^{man}-modified Eth (Eth-PEI^{man}) could be good vehicles for TCI.

Microspheres fabricated by electrospay have attracted much attention in recent years due to their good stability, slow and controlled release, simple preparation process [33–35]. The unique advantages of high surface area and porosity make nanofibrous patches a good drug-carrying substrate [35,36]. The combination of nanofibers and Eth-PEI^{man}-encapsulated microspheres may be a good solution to build ideal TCI patches in view of their remarkable properties on drug delivery and flexible adjustment of drug loading. Silk fibroin (SF) nanofibers have many applications due to their outstanding biocompatibility and skin affinity [13,36]. However, electrospun SF nanofibers are easily broken and fail

to meet the needs of practical applications, and thus they are blended with other polymers to improve their properties [37–41]. Polyvinyl alcohol (PVA) is a water-soluble synthetic polymer, non-toxic, biodegradable, and has good mechanical performance [40–42]. Besides, PVA has good spinnability and is suitable for blending with SF to prepare composite nanofibers by green electrospinning [40,41]. Therefore, the SF-PVA composite nanofibrous patches loaded with Eth-PEI^{man}-encapsulated microspheres could be a good choice for construction of TCI systems.

Tumor immunotherapy kills tumor cells effectively by activating the patient's immune system, and has the advantages of inhibiting tumor metastasis and recurrence and avoiding damage of normal cells [43]. Immune checkpoint blocker can eliminate immunosuppression and restart CTL effects in the tumor microenvironment [44,45]. Programmed death-1 (PD-1)/programmed death-ligand 1 (PD-L1) are considered the most promising target for tumor immunotherapy and anti-PD-1 monoclonal antibody (aPD-1) has been reported to cure advanced tumors such as gastric cancer, melanoma, lung cancer, and bladder urothelial cancer [43–45]. However, most patients are clinically insensitive to aPD-1 therapy [46,47]. To improve efficacy of aPD-1, many combination therapies have been reported in recent years [47–51]. A recent study has shown that the antitumor effects induced by aPD-1 requires "authorization" from DCs by expression of cytokines such as IL-12 [52], suggesting that DCs play a key role in the immune checkpoint blockade therapy. Furthermore, DCs are one of the best targets in cancer immunotherapies because of their potentials as APCs and their central role in coordinating innate and adaptive immunity [53]. The DCs-based vaccines can effectively trigger specific CD8⁺ CTLs through the antigen peptide-major histocompatibility complex class I (MHC-1) complexes and stimulate tumor killer production to prevent cancer from recurring [54,55]. Since there are abundant DCs in the skin tissues, we speculate that the combination of immune checkpoint blockers and DCs-targeted transcutaneous tumor vaccines (TTV) could achieve better antitumor efficacy.

In this study, a syngeneic mouse model for melanoma by subcutaneous injection of B16F10 cell lines was used to investigate the antitumor effect of the combination therapy with TTV and aPD-1. The complex of Eth-PEI^{man} was firstly fabricated and characterized to be used as carrier for TCI. The tyrosinase-related protein-2 peptide (SVYDFVWL) (termed as TRP2) was used as melanoma-specific antigen and encapsulated into the Eths, and CpGs as immune adjuvant adsorbed in PEI^{man} to obtain a TTV delivery vehicle complex (termed TRP2@Eth-PEI^{man}@CpGs). After confirming its ability to target and induce DCs maturation, the TRP2@Eth-PEI^{man}@CpGs was then mixed with polyvinylpyrrolidone (PVP) and sprayed into microspheres on the surface of electrospun SF-PVA composite nanofibers by electrospay to obtain composite nanofibrous patches loaded with TTV (termed TTVP). The transcutaneous performance and immune effect of the as-prepared TTVP was further evaluated. Finally, the in vivo antitumor efficacy of the combined treatment with TTVP and aPD-1 was explored using melanoma bearing mice.

2. Materials and methods

2.1. Materials

Lecithin, cholesterol, octadecylamine, PEI (Mw = 25 kDa), lithium bromide (LiBr), 1,10-dioctadecyl-3,3',30,30'-tetramethylindocarbocyanine perchlorate (DiI), bovine serum albumin (BSA), fluorescein isothiocyanate (FITC), Hoechst 33342 and Doxorubicin hydrochloride (Dox) were purchased from Sigma-Aldrich (Shanghai) Trading Co., Ltd (Shanghai, China). A-D-mannopyranosylphenyl isothiocyanate (MPITC) was pur-

chosen from MOLBASE (Shanghai, China). CpGs1826 (5'-TCCATGACGTTCTGACGTT-3') was synthesized by Synbio Technologies (Suzhou, China). The TRP2₁₈₀₋₁₈₈ (SVYDFVWL) were synthesized by Genscript (Nanjing, China). The PE-conjugated goat anti-mouse CD80 and CD86 monoclonal antibodies (clone No. are 16-10A1 and GL-1, respectively) and TMB ELISA kits (for detection of TNF- α , IFN- γ and IL-6) were purchased from Pepro Tech (USA), and aPD-1 (anti-mouse, clone: RMP1-14) from BioLegend, Inc (USA). Rat anti-mouse CD4 and CD8 (clone No. are #MAB0707 and #MAB0708, respectively) were purchased from Relia Tech (Germany). Cell counting Kit-8 (CCK-8) and Calcein-AM/PI Double Stain Kit and 4',6-diamidino-2-phenylindole (DAPI) were purchased from Shanghai YEASEN Biotechnology Co., Ltd (Shanghai, China). PVA and PVP were purchased from Shanghai Aladdin Biochemical Technology Co., Ltd (Shanghai, China). Cocoons of *B. mori* silkworm were from Huzhou Silk Co. (Huzhou, China). DMEM medium, RPMI-1640 medium and fetal bovine serum (FBS) were purchased from Gibco Life Technology Co., Ltd (USA). Ultrapure water was used throughout this study.

2.2. Cells and animals

L929 (mouse fibroblast cell line), B16F10 (mouse melanoma cell line) and mouse bone-marrow-derived dendritic cells (BMDCs) were used in vitro studies. L929 and B16F10 were obtained from the Institute of Biochemistry and Cell Biology, Chinese Academy of Science (Shanghai, China). BMDCs were isolated according to previous reports [13]. Briefly, the bone marrow cells were isolated from both shinbones and thighbones of C57BL/6 mice (4–5 weeks old) and cultured in RPMI-1640 complete medium (supplemented with 10% FBS, 100 μ g/mL streptomycin and 100 U/mL penicillin, 500 U/mL IL-4 and 1000 U/mL GM-CSF) in a humidified incubator of 5% CO₂ at 37 °C. After culture of one week, the suspended BMDCs were harvested. B16F10 and L929 were cultured in RPMI-1640 and DMEM respectively (both medium supplemented with 10% FBS, 100 U/mL penicillin and 100 μ g/mL streptomycin) at 37 °C in incubator with 5% CO₂.

Male C57BL/6 mice of 5 weeks were purchased from Shanghai SLAC Laboratory Animal Co. Ltd (Shanghai, China). The animals were maintained in a 12 h light/dark cycle with free access to food and water (SPF environment). All animal experiments were performed according to the guidelines approved by the Institutional Animal Care and Use Committee at Donghua University.

2.3. Preparation and characterization of Eth-PEI^{man}

PEI^{man} was prepared according to Ying Hu's method [30]. Briefly, 56 mg MPITC was dissolved in 10 mL methanol and this solution was added dropwise into PEI solution (108 mg PEI dissolved in 0.5 mL methanol) and stirred at room temperature to dissolve completely. The methanol was removed by evaporation at 30°C for 30 min. The residue was then dissolved in 5 mL of water and PEI^{man} was finally obtained after freeze-drying.

Eths were prepared according to the thin layer evaporation method [13]. Briefly, 100 mg lecithin, 10 mg cholesterol and 4 mg octadecylamine were sufficiently dissolved in 5 mL ethanol, and the solution was rotary evaporated to form a thin film. Then, the film was dissolved in 10 mL of H₂O/ethanol (7:3 in volume) containing PEI^{man} (1 mg/mL) or TRP2 (0.5 mg/mL) to obtain Eth-PEI^{man} or TRP2@Eth. TRP2@Eth solution mixed with equal volume of PEI^{man} (2 mg/mL) or PEI^{man}@CpGs solution (containing different amounts of CpGs) followed by gentle vortexing and further incubating at room temperature for 30 min to obtain TRP2@Eth-PEI^{man} or TRP2@Eth-PEI^{man}@CpGs solution containing different amounts of CpGs.

Nuclear magnetic resonance (NMR) spectra were recorded on a Bruker avance 500 using D₂O with tetramethylsilane as an internal reference. Infrared spectra were recorded on a Fourier-transform infrared (FTIR) spectrometer (Thermo Nicolet 6700, USA). KBr pellets of PEI and PEI derivatives were used in the infrared instrument. FTIR spectra were acquired after 16 scans between 4000 and 800 cm⁻¹. The morphology of the Eth, Eth-PEI^{man} and TRP2@Eth-PEI^{man}@CpGs were examined by transmission electron microscopy (TEM, JEM-2100F, jeol, japan). The zeta potential and particle size were measured by Zetasizer Nano ZS instrument (Malvern, UK). The encapsulation efficiency of Eth-PEI^{man} for TRP2 was determined by the method of ultracentrifugation.

2.4. Gel retardation and DNase resistance assays

DNA condensation ability of Eth-PEI^{man} was investigated using gel retardation assay. The plasmid DNA (pDNA)-encapsulated PEI^{man} (pDNA@PEI^{man}) were prepared at various ratios (0, 1, 5,10,15, 20) of nitrogen (of PEI^{man}) to phosphorus (of DNA) (N/P). The products were loaded on 1 % agarose gels with ethidium bromide (0.5 μ g/mL) and ran in TBE buffer at 90 V for 20 min. DNA retardation was visualized and photographed by a gel imager (FR-980B, Shanghai Furi Technology Co., LTD, China).

DNase I resistance assay was performed to assess the ability of Eth-PEI^{man} to protect DNA. Eth-PEI^{man}@pDNA complexes (N/P ratios of 15 and 20) were placed in DNase-free EP tubes, and 1 μ g of naked pDNA was used as control (two samples were set for each group). The samples were incubated with 2 μ L of DNase I for 1 h at 37°C, and then treated with EDTA for 10 min to inactivate DNase I. Subsequently, sodium dodecyl sulfate (SDS) was added to some of the samples. Finally, agarose gel electrophoresis (20 min at 90 V) was used to investigate changes of DNA content in each group.

2.5. Cytotoxicity assay

Cytotoxicity of Eth-PEI^{man} was investigated by cell proliferation assay. L929 cells were seeded into 96-well plates at a density of 1 \times 10⁴ cells/well cultured for 24 h. Then, different concentrations of Eth-PEI^{man} were added and incubated for another 24 h. Subsequently, medium was then washed with sterile PBS buffer for 3 times, and 100 μ L fresh RPMI 1640 medium (without FBS) containing 10 μ L CCK-8 reagent was added into each well and incubated for 1 h at 37 °C. Finally, a microplate reader (Multiskan MK3, Thermo, USA) was used to record the absorbance at 450 nm (the absorbance of cells without treatment used as a control). The relative cell viability (%) was calculated by the following equation:

$$\text{Cell Viability (\%)} = (\text{At}-\text{Ab})/(\text{Ac}-\text{Ab}) \times 100\%$$

(At: absorbance of the tested samples; Ab: absorbance of the blank wells containing culture medium and CCK-8 solution but without cells; Ac: absorbance of the controls).

To image the above treated cells, the medium was discarded and washed three times with PBS. Then, 100 μ L of calcein-AM/PI solution was added to the wells and incubated for 15–20 min in the dark. Subsequently, the staining solution was discarded and cells were washed with PBS. Finally, the cells were observed and photographed using a fluorescence microscope (DMi 8, Leica, Germany).

2.6. Assays for targeted induction of DCs in vitro

2.6.1. Phagocytosis

To observe the DCs-targeted performance of Eth-PEI^{man}, Dil-labeled Eth-PEI^{man} (15 μ g/mL) was used to treat BMDCs seeded in six-well plates (1 \times 10⁵/well) for 2 h at 37°C. After washing three

times with PBS, the cells were fixed with 4% paraformaldehyde for 30 min. Cells were then stained with DAPI and observed with a fluorescence microscope (DMI 8). The fluorescence intensity of different samples was compared and analyzed by ImageJ 1.44 software (National Institutes of Health, USA). To investigate the DCs-targeted drug delivery performance of Eth-PEI^{man}, BMDCs were co-cultured with free Dox or Dox-loaded carriers (Dox@Eth, Dox@Eth-PEI^{man}) for 24 h at 37°C (the cells treated with equal volume of PBS were used as control). The cells were washed three times with PBS to remove redundant complexes and re-suspended in 300 μ L PBS. Finally, the samples were examined with flow cytometry under a FACSCalibur (Becton Dickinson, USA) to quantify the fluorescence of Dox.

2.6.2. Evaluation of DCs maturation

To assess the maturation of DCs in response to the Eth-PEI^{man} loaded with antigen and adjuvant, BMDCs were incubated in six-well plates (2×10^5 /well) with TRP2 or/and CpGs (free or encapsulated in the carriers) for 24 h at 37°C (the cells treated with equal volume of PBS were used as negative control). The cells were washed three times with PBS and re-suspended in 100 μ L PBS containing 1 μ g PE-goat anti-mouse CD80 or CD86 monoclonal antibodies and incubated at 4°C in the dark for 20 min. After washing three times with PBS, the cells were re-suspended in 300 μ L PBS and their expression levels of CD80 and CD86 were detected with flow cytometry.

2.7. Preparation of the TTVP

Raw silk fibers were degummed three times with 0.5% (W/V) Na₂CO₃ solution for 30 min at 100°C and then rinsed with warm distilled water. After drying, degummed silk was dissolved in 9.3 M LiBr at 45°C for 1 h to obtain a homogeneous solution. After dialysis (MWCO of dialysis bag is 14000 KDa) at room temperature for three days against water, the solution was filtered and lyophilized to obtain regenerated SF sponges.

SF solution was concentrated to 6% (w/v) before the electrospinning step. 8% (w/v) PVA solution was prepared by dissolving PVA in hot water (T = 90 °C) for about 3 h. Different ratios of SF and PVA solutions were mixed and stirred at room temperature for 12 h. The mixed solution was then transferred to a syringe and electrospun onto aluminum foil with a rate of 1.0 mL/h at a voltage of +15 kV and a collect distance of 15 cm. The resulting products were dried and stored in a desiccator for further use in the electro-spray step. 1 g PVP was dissolved in 5 mL ethanol/H₂O (6:4 in volume) and mixed with equal volume of drug-loaded Eth-PEI^{man} solution. The mixture was then transferred to a syringe and electro-sprayed onto the SF-PVA composite nanofibrous matrices fixed on the receiving plate with a rate of 1.0 mL/h under +18 kV at the collect distance of 15 cm, and the humidity was set 8%. Surface morphology of the product was observed by SEM (JEOL, JSM-5600, Japan) after sputter-coating by gold at 7 mA for 60 s. The sizes of the microspheres and the nanofibers were analyzed by ImageJ 1.44 software.

2.8. In vitro skin permeation assay

The transdermal performance of the TTVP was examined by Franz vertical diffusion method using FITC-labeled BSA (fBSA) and Hoechst 33342-labeled plasmid DNA (hpDNA) as the model drugs. To imitate the physiological environment of the human body, PBS buffer was used as receiving liquid and temperature was set to 33°C. After the ICR mice were sacrificed by necking, the abdomen of the mice was shaved and the skin was carefully removed from the abdomen. The intact skin was placed on the receiving pool (the dermis tightly contacted with PBS buffer). 2 mL of receiving

solution was obtained and supplemented with the same volume of fresh PBS at each sampling time point. All samples collected from the receiving solution were measured (at 490 nm for fBSA, 354 nm for hpDNA) using a UV-vis spectrophotometer (UV1100, TECHCOMP, China). The cumulative release of drugs is calculated according to the following formula:

$$Q = \frac{VCn + \sum_{i=1}^{n-1} CiVi}{Q'} \times 100\%$$

Where Q is the cumulative amount of drug released, V is the volume of the diffusion pool, Ci is the drug concentration at the i time sampling, Vi is the volume at the i time sampling and Q' is the actual amount of drug contained in the Eth.

After transdermal administration for 24 h, the skin was dehydrated, paraffin-embedded and sequentially sectioned. Fluorescence distribution in the skin was observed using fluorescence microscopy (DMI 8).

2.9. Detection of the TTVP-induced cytokines

The mice were anesthetized by intraperitoneal injection of 0.1 mL 1% pentobarbital solution. Then, the abdomen hair of each mouse was removed. After moistened the abdomen skin with a little PBS, the as-prepared TTVP (2 cm \times 2 cm, the actual loading amounts for TRP2 and CpGs were about 125 μ g and 12.56 μ g, respectively) was attached to the abdomen (drug-loaded microspheres against the skin) and fixed with medical tape for 3 days. The same operation was repeated on the 14th day to boost the immunization. Non-administered mice served as control. Blood samples were collected from eye venous plexus (0.5 mL for each mouse) on day 10 or day 24, respectively. Serum were isolated from the blood samples by further standing for 30 min at RT and then centrifugation for 5 min at 3000 rpm. Finally, TNF- α and IL-12 were detected according to the instructions of ELISA kits. Levels of TNF- α and IL-6 in the skin where the vaccine is applied for 24 hours were also measured by ELISA after the skin samples being homogenized and filtered.

2.10. Evaluation of the antitumor effect of TTVPs and aPD-1

Mice were randomly divided into four groups (5 mice in each group): TTVP, TTVP + aPD-1, aPD-1, and blank control. For TTVP treatment, mice were transcutaneously immunized with the method described above. For aPD-1 treatment, mice were injected subcutaneously with aPD-1 (20 μ g/mouse) on the 1st day and the 14th day respectively. For control group, the mice were not treated. On the 21st day, all the mice were subcutaneously inoculated B16F10 cells (1×10^6 cells/mouse, suspended in 100 μ L PBS) on the right hind legs. Growth of the tumors was observed every day after inoculation, when the tumors can be observed and measured (the day was defined as day 0), the length (L) and width (W) of the tumors were measured with a vernier caliper every 3 days. Tumor volume (V) was calculated using the equation: $V = 0.5 \times L \times W^2$. Mice weight were also measured and recorded.

To investigate the microenvironment of tumor tissue, all the mice were sacrificed on day 18 (based on day 0) and the tumors were taken out and fixed with paraformaldehyde. After staining with hematoxylin-Eosin (H&E), TUNEL, anti-CD4 (clone: #MAB0707) or anti-CD8 (clone: #MAB0708), respectively, the tumor tissues sections were examined microscopically and the fluorescence intensity of different samples was analysed using ImageJ 1.44 software.

To investigate the safety of the above immunotherapy, heart, liver, spleen, lung and kidney were collected from the above sacrificed mice and fixed with paraformaldehyde. Then, paraffin sec-

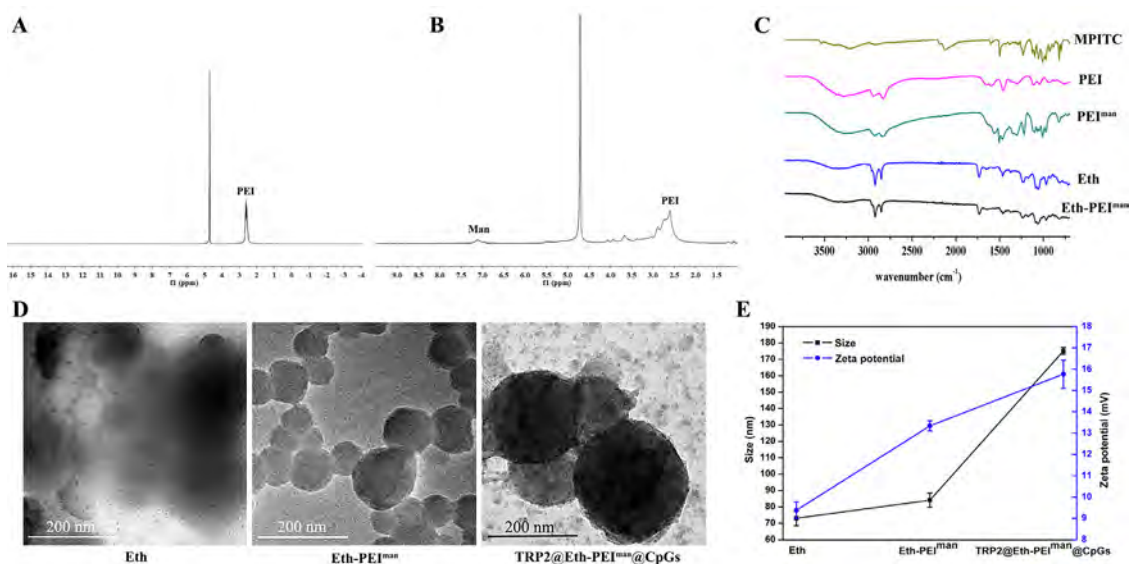


Fig. 1. ^1H NMR spectra of PEI (A) and PEI^{man} (B), FTIR spectra (C), TEM images (D), size and Zeta potentials (E, data are expressed as mean \pm SD, n=3) of the carriers.

tions of the organs were made and stained with H&E. Finally, the sections were examined microscopically (DMi 8).

2.11. Statistical analysis

All experiments were conducted at least three times, and numeric data were expressed as mean \pm standard deviation (SD) unless otherwise indicated. Statistical significance was analyzed by one-way analysis of variance (ANOVA) with Tukey's post hoc test. A p value less than 0.05 was considered significant.

3. Results

3.1. Characterization of Eth-PEI^{man}

The ^1H NMR spectrum of PEI^{man} shows characteristic signals of the mannose group and PEI (Fig. 1A & B). The large peak at 4.5–5.0 ppm represents water. The peak at 2.4–2.8 ppm represents the H-carbon unit in the PEI backbone and signal at 7.1 ppm represents the phenyl group in mannose [30–32]. FTIR spectra of PEI and MPITC show that the $-\text{N}=\text{C}=\text{S}$ band of MPITC disappeared from the PEI^{man} spectrum at 2125 cm^{-1} , indicating that the isothiocyanate group on MPITC has been successfully conjugated to the amine group of PEI [30–32] (Fig. 1C a, b, c). This result was also confirmed by a new absorption peak at 1508 cm^{-1} , which belongs to the phenyl group on phenyl isothiocyanate [30–32]. The Eth-PEI^{man} spectrum shows signal peaks at 2927 cm^{-1} and 2857 cm^{-1} corresponding to groups of the Eth. The characteristic absorption peaks of cholesterol at 1378 cm^{-1} and 1467 cm^{-1} were weakened due to the attachment of PEI^{man} (Fig. 1C d&e). These results indicate that mannose and PEI are successfully linked to Eth. Since hydrogen bonds and van der Waals forces can be formed between the amino group of PEI and the phospholipid group of Eths, PEI and Eths are more likely bounded by hydrogen bonds and van der Waals forces. TEM images show that the Eth has a multi-layered cystic structure with uniform size and clear outline, while the Eth-PEI^{man} is approximately spherical and its size increases significantly when both Eth and PEI load drugs (Fig. 1D). The potential of Eth increased by about 4 mV with the modification of PEI^{man} and continue to increase after loading TRP2 and CpGs (Fig. 1E). The particle size and potential of Eth-PEI^{man} change with the N/P value, bigger value result in smaller particle size and higher potential

(Fig.S1). As shown in Fig.S1, the ability of Eth-PEI^{man} to condense DNA became stronger when N/P value increase, and the optimal N/P value between PEI^{man} and DNA is 15, at this value Eth-PEI^{man} can load more DNA and protect them from the digestion of DNase I. The encapsulation efficiency of Eth-PEI^{man} for TRP2 (TRP2@Eth) was $66.16\%\pm 3.16\%$, while for CpGs (CpGs@PEI^{man}) was 100% at a N/P value of 15 or more.

3.2. Cytotoxicity of Eth-PEI^{man}

The cytotoxicity of the carriers was investigated with L929 cells. After treated with different carriers, the viabilities of L929 cells were determined by CCK-8 assay. As shown in Fig. 2A, the carriers had good cytocompatibility at concentrations of less than $15\text{ }\mu\text{g}/\text{mL}$. When the concentration reached to $15\text{ }\mu\text{g}/\text{mL}$ or more, PEI^{man} showed significant cytotoxicity, while the bare Eth showed a much better cytocompatibility. The performance of Eth-PEI^{man} is between Eth and PEI^{man}, showing significant cytotoxicity at the concentration of $20\text{ }\mu\text{g}/\text{mL}$ or above. The fluorescence images of the cells treated with carriers of $15\text{ }\mu\text{g}/\text{mL}$ showed a similar result with that of CCK-8 (Fig. 2B). Based on these results, the working concentration of Eth-PEI^{man} was set to $15\text{ }\mu\text{g}/\text{mL}$ in the subsequent experiments.

3.3. DCs-targeted ability of Eth-PEI^{man}

To examine the targeting ability of Eth-PEI^{man} towards DCs, we labelled the Eths with the red fluorescent dye DiI and monitored their phagocytosis by DCs. As shown in Fig. 3, the phagocytosis of Eth-PEI^{man} is more effective than that of the bare Eths, which suggests that the existing of PEI^{man} significantly improved the ability of the carriers to target DCs. To further confirm the DCs-targeted ability of Eth-PEI^{man}, the phagocytic efficiency of the carriers loaded with drugs (Dox was used as model drugs) was investigated by flow cytometry. The results show that drugs encapsulated within the Eths are more easily taken up by DCs than free ones (Fig.S2). Moreover, Eth-PEI^{man} shows a much better performance on delivering drugs into DCs than the bare Eths do (Fig.S2), which is consistent with the result in Fig. 3 and confirm the ability of Eth-PEI^{man} to target DCs.

TRP2@Eth-PEI^{man}@CpGs was prepared as a transcutaneous anti-melanoma vaccine. The ability of TRP2@Eth-PEI^{man}@CpGs to in-

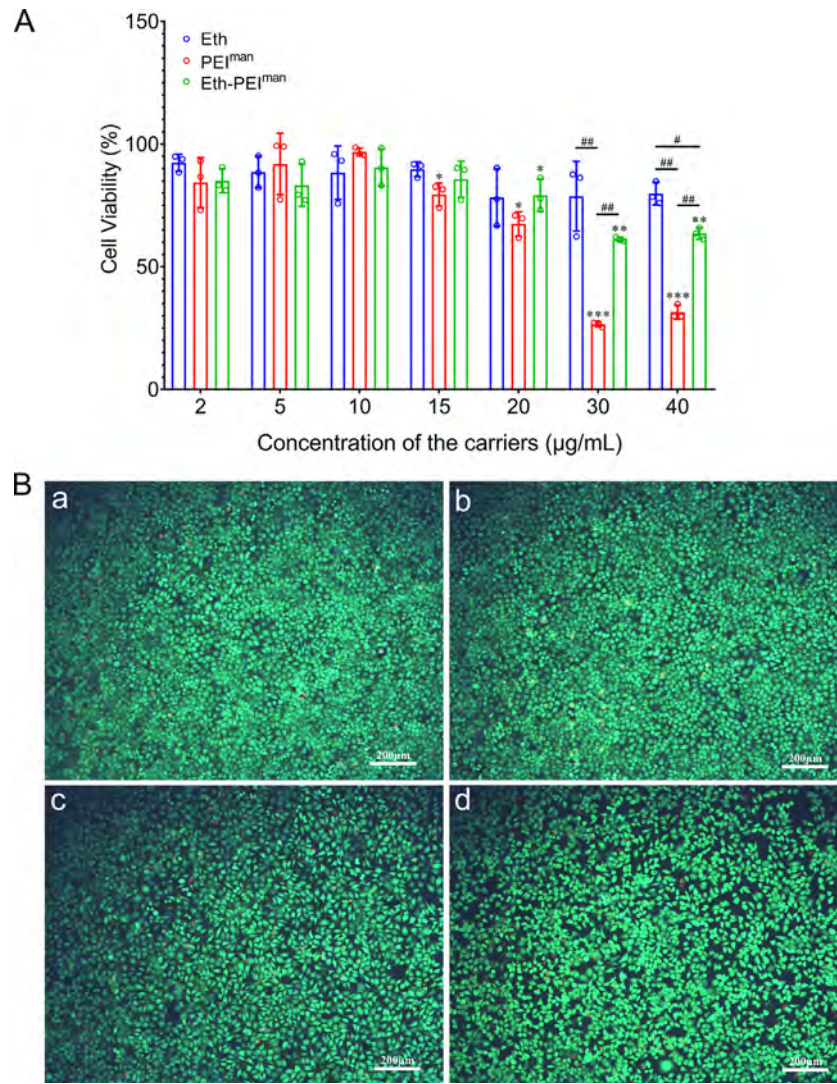


Fig. 2. Cytotoxicity data of the carriers (A: viabilities of L929 cells co-cultured with the carriers at different concentrations for 24 h; Data are expressed as mean±SD, n=3; * p < 0.05, ** p < 0.01, *** p < 0.001, compared with control whose value is set as 100%; # p < 0.05, ## p < 0.01; B: fluorescence images of L929 cells treated with the carriers of 15 µg/mL for 24 h; a: control; b: Eth; c: Eth-PEI^{man}; d: PEI^{man}).

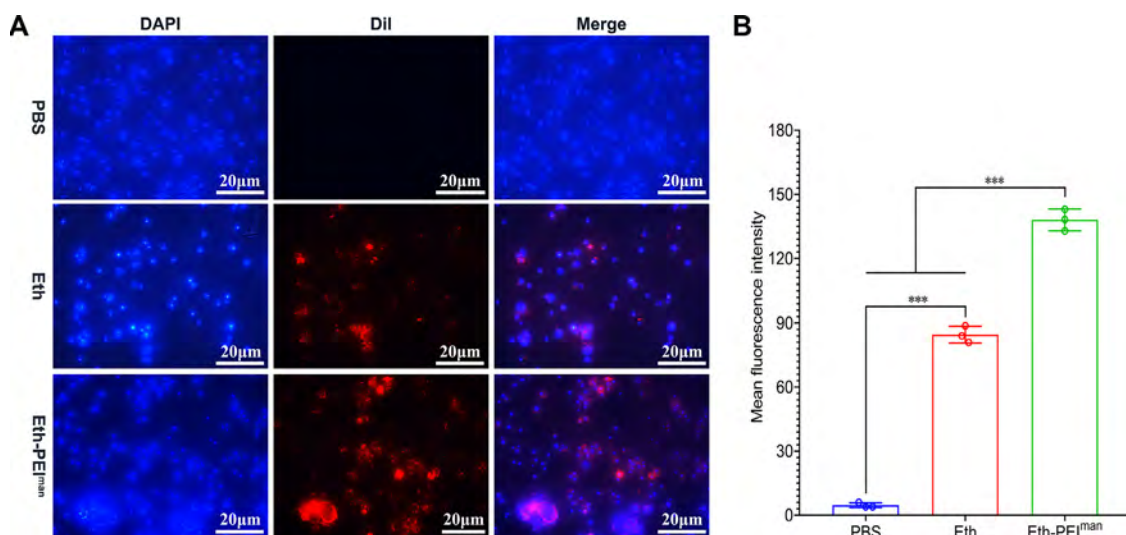


Fig. 3. Fluorescence micrograph of BMDCs after co-cultured with the carriers for 2 hours (A) and their quantitative analysis (B, data are expressed as mean±SD, n=3, *** p < 0.001)

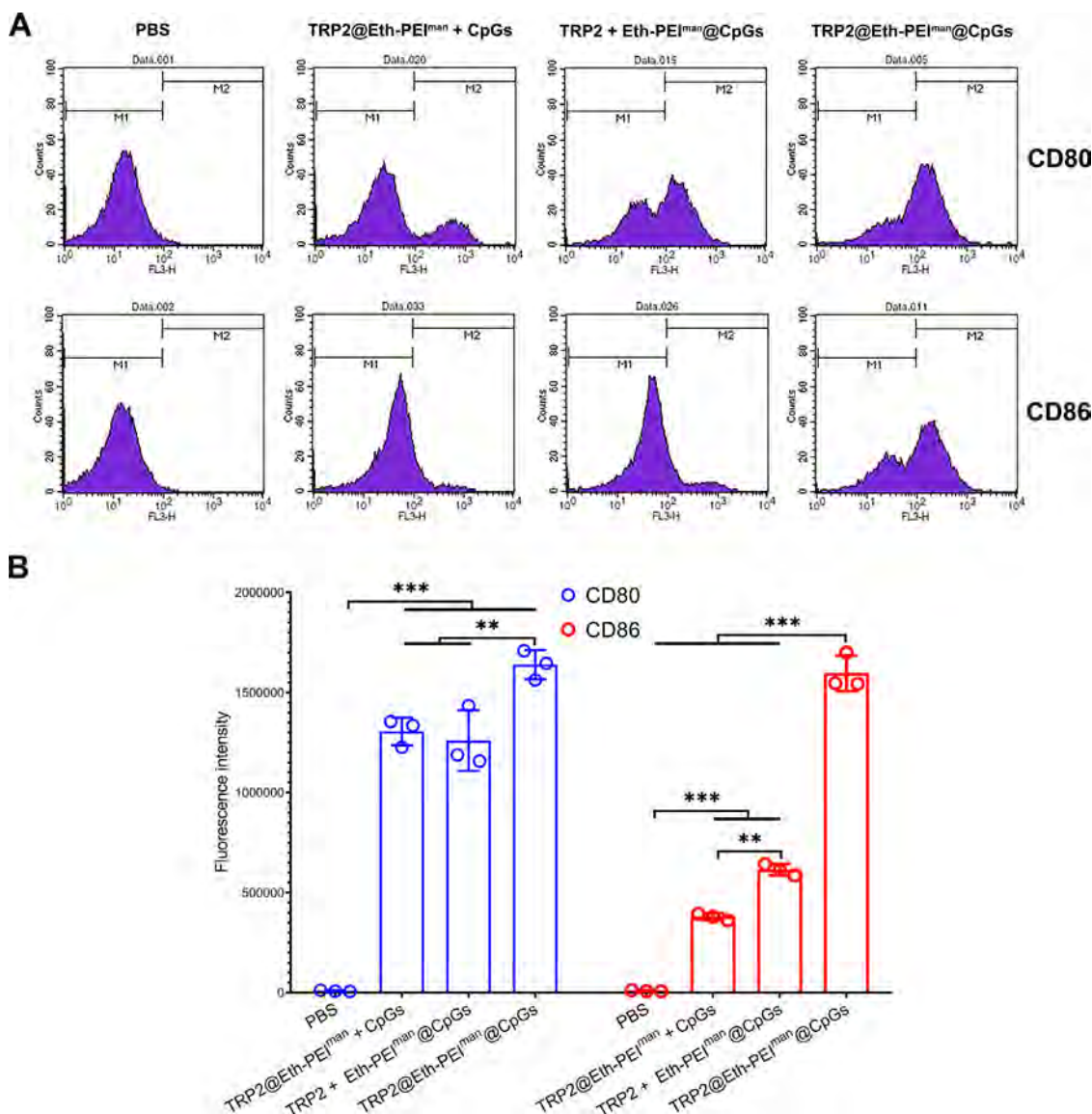


Fig. 4. The levels of CD80 and CD86 expressed by BMDCs treated with TRP2 and CpGs (A: Flow cytometry histograms; B: Quantitative analysis of the flow cytometry histograms (data are expressed as mean±SD, n=3; ** p < 0.01, *** p < 0.001)

duce the maturation of DCs was evaluated by detecting the expression of CD80 and CD86, markers of DCs maturation. As shown in Fig. 4, the expression levels of CD80 and CD86 were significantly up-regulated in DCs following the stimulation of TRP2 or/and CpGs compared with the control. Moreover, the levels of the markers induced by TRP2@Eth-PEI^{man}@CpGs is the highest, confirming the higher efficiency of Eth-PEI^{man} to deliver antigen and adjuvant to DCs. Furthermore, much more CD86⁺ cells were observed in the skin of the mice after transcutaneous administration with TRP2@Eth-PEI^{man}@CpGs for 24 hours (Fig.S3), suggesting the maturation of many DCs in vivo. These results indicate that TRP2@Eth-PEI^{man}@CpGs can effectively promote the phenotypic maturation of DCs.

3.4. Characterization of the TTVP

3.4.1. Morphology

The TTVP were obtained by electrospaying PVP microspheres containing TRP2@Eth-PEI^{man}@CpGs onto the green electrospun SF-PVA composite nanofibers. As shown in Fig. 5, SF-PVA nanofibers showed a round and smooth morphology with a diameter of

342.14±82.37 nm. The mechanical performance of the composite nanofibers was significantly improved compared with that of the neat SF nanofibers (Fig. S4). The microspheres have a round and smooth shape with a particle size of 622.45±108.43 nm, they were evenly distributed on the surface of the SF-PVA nanofibers in the TTVP.

3.4.2. Transdermal performance

In vitro transdermal experiments were used to examine whether the TTVP could transcutaneously release the encapsulated drugs. As shown in Fig. 6, the biomacromolecules (fBSA and hpDNA) was released against the skin effectively with the help of Eth-PEI^{man}. The cumulative release percentage of DNA was higher than that of BSA(Fig. 6A), which is in line with their different encapsulation efficiency. To further assess the transdermal performance of the composite nanofibrous patches, the retention and distribution of the drugs in the skin were investigated (Fig. 6 B&C). The fBSA- and hpDNA-loaded carriers (fBSA@Eth-PEI^{man}@hpDNA) were clearly shown distribution in the dermis of the skin, presenting a typical ring structure of blue outer circle and green inner circle (Fig. 6C). The transdermal experiment with Dox as model drug

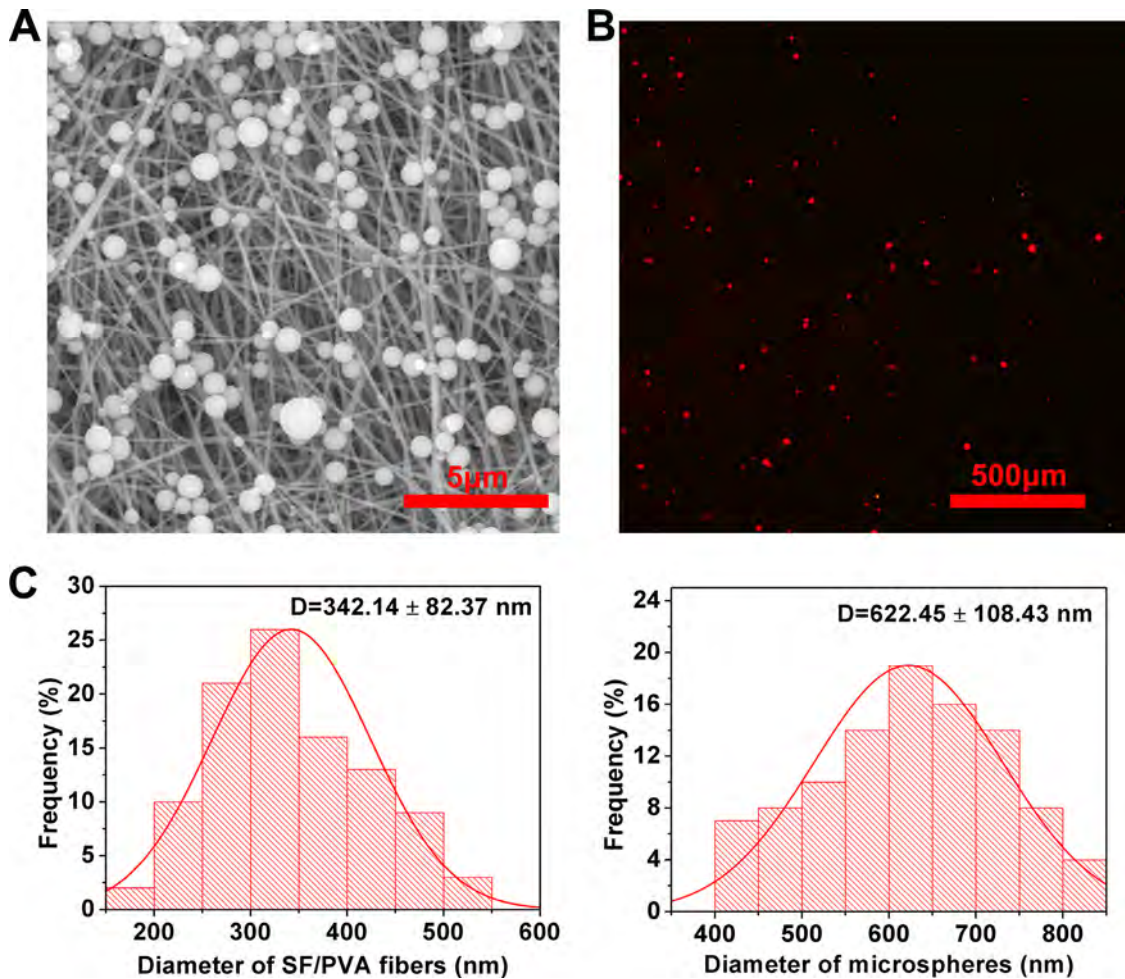


Fig. 5. Morphology of TTVP (A: SEM micrograph; B: fluorescent photograph, the red fluorescence refers to DiI-labeled Eth-PEI^{man}; C: diameters of the microspheres & nanofibers, data are expressed as mean±SD, n=100)

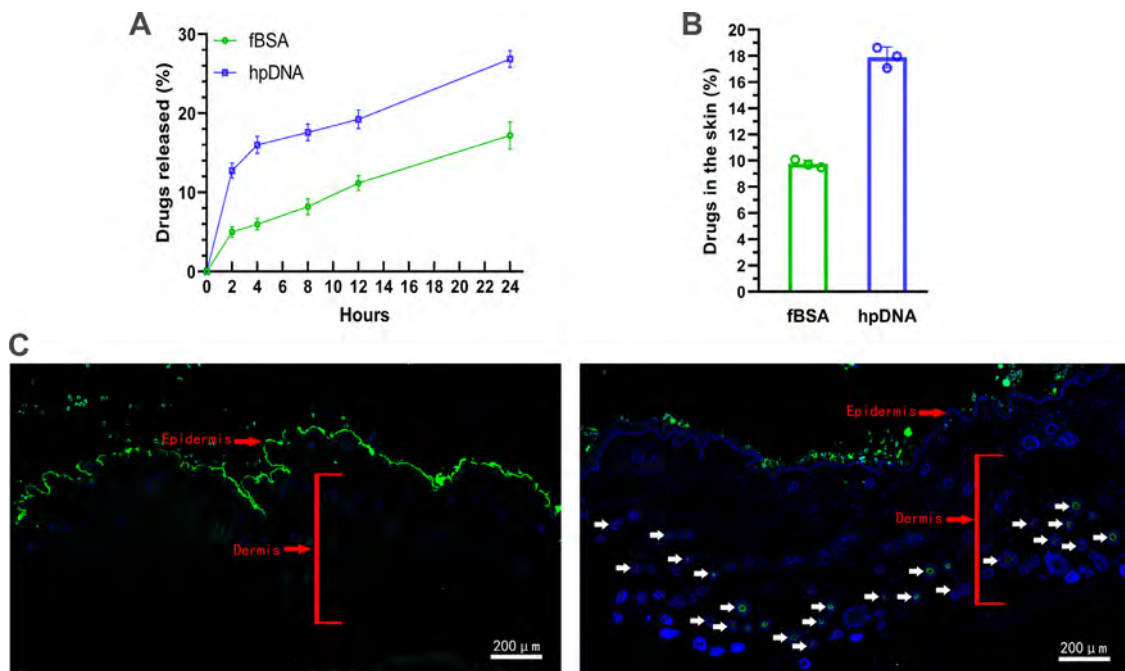


Fig. 6. In vitro transdermal drug release data (A: cumulative release curve (Data are expressed as mean±SD, n=3; B: retention in the skin (Data are expressed as mean±SD, n=3); C: micrograph of the skin tissue sections after transdermal experiment (left: free drugs-loaded SF-PVA nanofibrous patch; right: fBSA@Eth-PEI^{man}@hpDNA-loaded SF-PVA nanofibrous patch; fBSA: FITC-labeled BSA; hpDNA: Hoechst 33342-labeled plasmid DNA; green refers to fBSA, blue refers to hpDNA, the white arrows indicate fBSA@Eth-PEI^{man}@hpDNA which clearly presents a structure of blue outer circle and green inner circle)

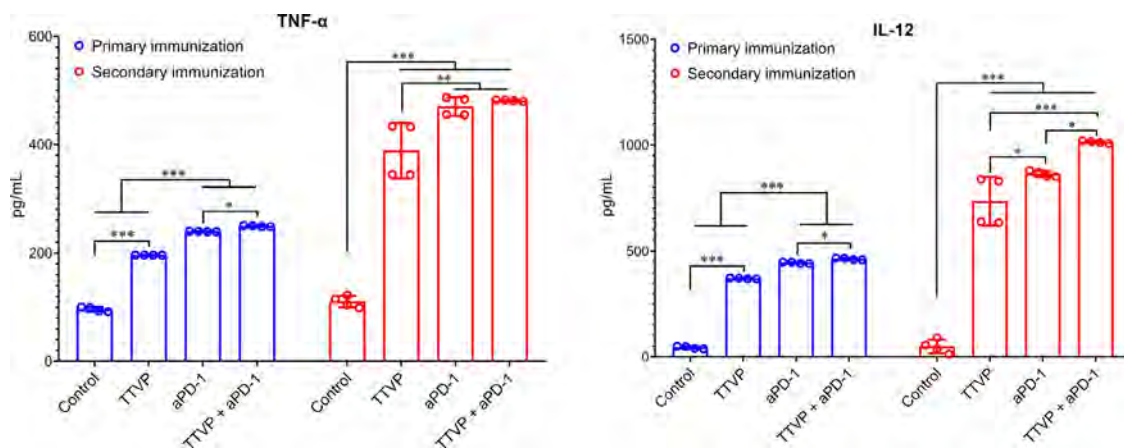


Fig. 7. The secretion levels of serum TNF- α and IL-12 after different treatment in mice (Data are expressed as mean \pm SD, n=4; * p < 0.05, ** p < 0.01, *** p < 0.001).

showed that the presence of Eth is critical to the transdermal performance of the carrier complex (Fig.S5). These data indicate that the Eth-PEI^{man} loaded nanofibrous patch has a good transdermal drug release performance.

3.5. Expression of cytokines induced by the TTVP

The levels of IL-6 and TNF- α in the local skin where the TTVP was applied for 24 hours were detected by ELISA. The results showed that administration of TTVP significantly enhance the skin levels of both IL-6 and TNF- α (Fig.S6), confirming that TRP2 and/or CpGs encapsulated in the TTVP were successfully delivered into the skin to stimulate inflammatory reaction. The serum levels of TNF- α and IL-12 was further detected to investigate whether TTVP can induce an effective immune response. As shown in Fig. 7, the administration of TTVP or aPD-1 induced significantly higher secretion levels of TNF- α and IL-12 than the negative control did. Interestingly, the combination treatment with TTVP and aPD-1 induced more expression of the cytokines than monotherapy did. These results indicate that both TTVP and aPD-1 can effectively activate the immune response.

3.6. Antitumor effect of the combined treatment with TTVP and aPD-1

The antitumor activity of the TTVP was evaluated using a syngeneic mouse model for melanoma by subcutaneous injection of B16F10 cell lines. After treatment with TTVP, mice were injected with B16F10 cells in their legs, and the growth of melanoma was measured. As shown in Fig. 8, the tumor volume of mice in each group gradually increased with time, and the slowest tumor growth was in the group of combination therapy with TTVP and aPD-1 (Fig. 8B, E & Fig.S7). On day 18, the tumor was isolated from the mice and weighted. As shown in Fig. 8 C, the change in tumor mass is consistent with the change in tumor volume. The tumor mass of the untreated control was significantly larger than those in the treatment groups (Fig. 8C). Also, the weight changes of the mice during the experiment were measured and recorded to evaluate the tumor growth of mice more objectively. The body weight of the mice in the combination therapy group did not change significantly (Fig. 8D), which is consistent with the tumor growth trend. The effect of different treatments can also be visually seen from the photo of tumor-bearing mice and tumors on day 18 (Fig. 8E & Fig.S7). These results indicate that TTVP treatment has the same good tumor inhibition as aPD-1 therapy. Moreover, the combined application of TTVP and aPD-1 showed a much stronger inhibitory

effect on tumor growth than TTVP or aPD-1 monotherapy, suggesting that there is a synergistic antitumor effect between the two treatments.

The tumor tissues of different treatment were investigated after H&E, TUNEL and immunohistochemistry staining (Fig. 9). As shown in Fig. 9A, the tumor cells are closely packed and the blood vessels are abundant in the tissue from the untreated control group, showing the typical pathological characteristics of the tumor. While the tumor tissues from the treatment groups showed large areas of white and tan, which represents the areas of tumor necrosis, and the combination treatment group had the largest area of necrosis. The TUNEL staining (it stains apoptotic cells green) of the tumor tissues showed that the green fluorescence intensity of the combined treatment group is significantly higher than that of the other groups, followed by the aPD-1 or TTVP monotherapy groups (Fig. 9). Anti-CD4 and CD8 immunohistochemical staining showed that there were more CD4⁺ and CD8⁺ T cells in the tumor tissues of the treatment groups compared with the control, indicating that TTVP or/and aPD-1 induced cytotoxic T lymphocyte (CTL) responses. Also, the combination therapy of TTVP and aPD-1 resulted in much more T cells infiltration in the tumor tissue than the monotherapy did, which is consistent with the data of tumor size. These data suggested that the TTVP or/and aPD-1 treatment may significantly inhibit tumor growth by enhancing the infiltration of CD4⁺ and CD8⁺ T cells in tumor tissues and thereby mediating tumor cell apoptosis, during which the two treatments can produce a synergistic effect through certain mechanisms.

3.7. Biosafety of the TTVP

The safety of the treatments can be evaluated by histological observation of the important organs of the treated mice. As shown in Fig. 10, there is no significant difference between the treatment groups and the blank control. The hearts, lungs, kidneys, livers and spleens from the mice showed normal cell morphology and there were no inflammatory cell infiltration or other lesions. Therefore, the treatment of TTVP or/and aPD-1 has a good biosafety.

4. Discussion

The key of TCI is to deliver antigen molecules through the dense cuticle and target DCs. Many studies have proved that Eth is a useful carrier for transdermal drug delivery [8–12]. Due to the presence of C-type lectin receptors on the surface of DCs, the carriers modified with galactose or mannose have the ability of targeting DCs [14–16]. We recently reported that the electrospun SF

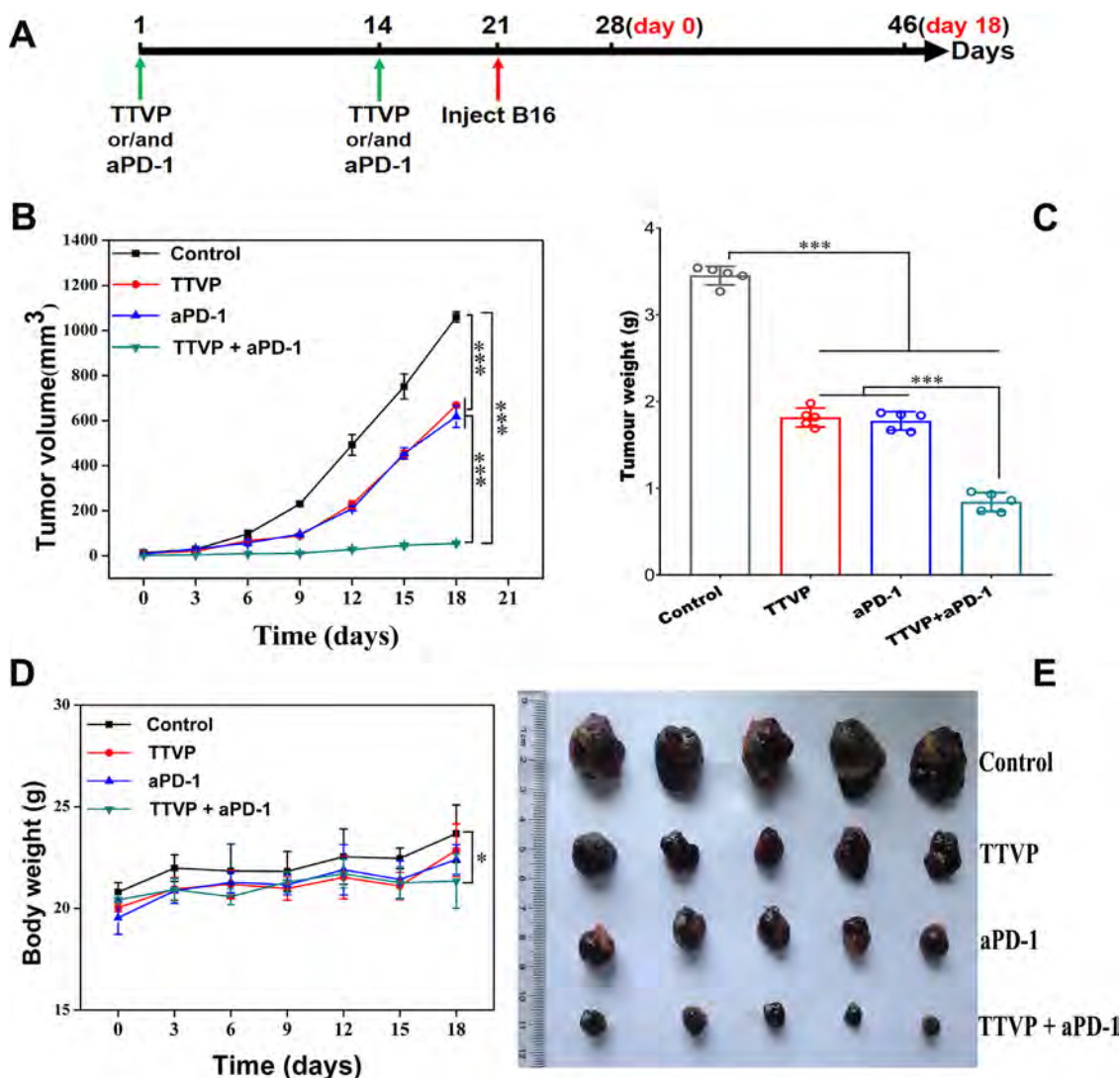


Fig. 8. Schematic illustration of in vivo antitumor experiment (A), tumor volume changes (B), average weight of tumors at day 18 (C), Body weight changes of tumor-bearing mice (D) and photograph of the tumors at day 18 (E) (Data are expressed as mean \pm SD, n=5; * $p < 0.05$, *** $p < 0.001$).

nanofibrous patches loaded with galactose-modified Eths can effectively deliver macromolecular antigens to DCs through transdermal route and successfully trigger cellular and humoral immune responses [13]. Since the combination of antigen and adjuvant can significantly enhance the immune response, co-delivery of peptides and CpGs to APCs is an innovative method in tumor immunotherapy [21,56,57]. Here, we report a TCI system based on SF-PVA nanofibers and Eth-PEI^{man} that simultaneously loads peptide antigens and CpGs (antigen molecules are encapsulated in Eth and CpGs are adsorbed in PEI^{man}), and explore its anti-tumor activity by using mouse melanoma as a model (TRP2₁₈₀₋₁₈₈ used as antigen).

The particle size and potential of Eth-PEI^{man} were both larger than Eths due to the existence of PEI^{man} (Fig. 1). Positively charged carriers are easier to adhere to the negatively charged cell membrane, which makes them better candidates for drug delivery. A smaller particle size is also conducive to endocytosis. The optimal N/P value of PEI^{man} against DNA was set to 15, under this condition, Eth-PEI^{man} can effectively protect CpGs from being degraded by DNase and maintain a relatively small particle size (Fig. S1). Results of cell experiments showed that Eth-PEI^{man} has good cytocompatibility at a concentration of less than 20 μ g/mL (Fig. 2). Eth-PEI^{man} also showed a good ability to target DCs as demon-

strated by the phagocytosis experiments (Fig. 3). The presence of PEI^{man} significantly increased the phagocytosis rate of drugs loaded in the Eths (Fig.S2), which further proves that PEI^{man} can target and bind DCs. In vitro experiments showed that TRP2@Eth-PEI^{man}@CpGs has more powerful ability to stimulate DCs maturation than the free antigens and CpGs do (Fig. 4). The maturation of DCs induced by TTVP was also confirmed by the data of in vivo (Fig.S3). TRP2₁₈₀₋₁₈₈ has been proven to be an effective inducer of antitumor immunity, it can induce large number of tumor-reactive T cells in melanoma patients [58,59]. CpGs has strong immunostimulatory properties, it can be recognized and captured by the DEC-205 receptor on the surface of DCs, and activate the TH1 response through the TLR9 signaling pathway [21–23]. Therefore, TRP2@Eth-PEI^{man}@CpGs can be a good anti-melanoma transcutaneous vaccine.

With high specific surface area and porosity, the electrospun nanofibrous patches have unique advantages as substrate of drug delivery [35–36,60]. By one-step electrospinning, Yang et al. prepared SF nanofibrous patches loaded with Eths, which could effectively deliver antigens and induce immune responses via transdermal route [13]. However, this one-step method for preparing transdermal drug delivery patches has two limitations: 1) Drug loading is limited because the addition of Eths has a greater in-

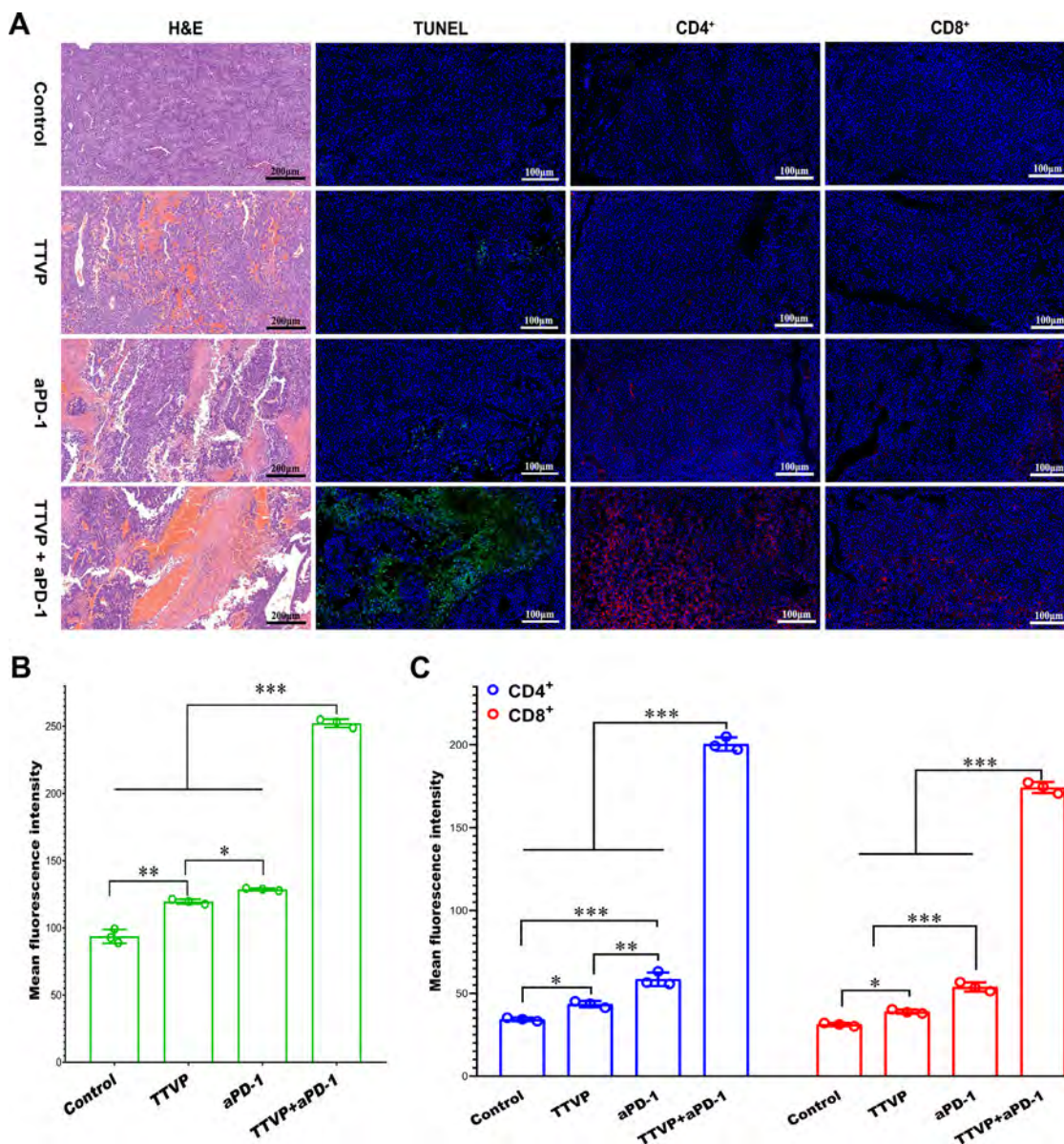


Fig. 9. Micrographs of tumor tissues stained by H&E, TUNEL and antibodies of CD4/CD8 (A), fluorescent intensity of TUNEL (B) and CD4/CD8 (C) staining (Data are expressed as mean±SD, n=3; * p < 0.05, ** p < 0.01, *** p < 0.001).

fluence on the electrospinning process (high concentration of Eths causes spinning failure); 2) The drug-carrying Eths are embedded in the fibers, which may affect the release of drug to a certain extent. In this study, the transcutaneous drug delivery patches obtained by spraying microspheres (containing drug-loaded Eth-PEI^{man}) onto nanofibers using electrospay ideally overcomes the above-mentioned drawbacks: the drug loading can be flexibly controlled by the time of electrospay (Fig.S8); the drug-loaded microspheres are distributed on the surface of the nanofibers, easier to contact and penetrate the epidermis. In addition, SF-PVA composite nanofibers with better mechanical properties was used to replace pure SF nanofibers in this study (Fig.S4), which is conducive to practical application. PVP is easily soluble in water and has good biocompatibility [61]. It is easy to obtain drug-loaded microspheres by mixing PVP and drug-carrying Eths through electrospay. In this study, the microspheres containing TRP2@Eth-PEI^{man}@CpGs were sprayed onto the SF-PVA nanofibers to obtain TTVP (Fig. 5). When in use, the TTVP is applied to the pre-moistened local skin so that it fits closely with the skin. Since PVP is very soluble in water,

the drug-carrying Eth-PEI^{ma} can be quickly released from the microspheres and contact with the skin. In vitro transdermal experiments proved that the microspheres-loaded nanofibrous patches have good performance in delivering biomacromolecules into deep layers of the skin by transdermal route (Fig. 6). Therefore, the developed TTVP in this study has good performance in transcutaneous delivery of antigens and adjuvants to DCs, showing a good application potential in tumor treatment.

The transdermal efficiency of free biomacromolecules is much lower than those encapsulated in the Eths, which has been proved by our previous study [13]. Thus, we did not set up a free TRP2 and/or CpGs as control groups in animal experiments. We mainly focused on investigating the anti-melanoma effect of TRP2@Eth-PEI^{man}@CpG and whether it has a synergistic antitumor effect with aPD-1 in this study. The immune activity of TTVP was verified by the increased levels of cytokines. The application of TTVP significantly promoted the expression of cytokines in both the skin (IL-6 and TNF-α) (Fig.S6) and serum (IL-12 and TNF-α) (Fig. 7). The levels of cytokines such as IL-6, TNF-α and IL-12 are useful indi-

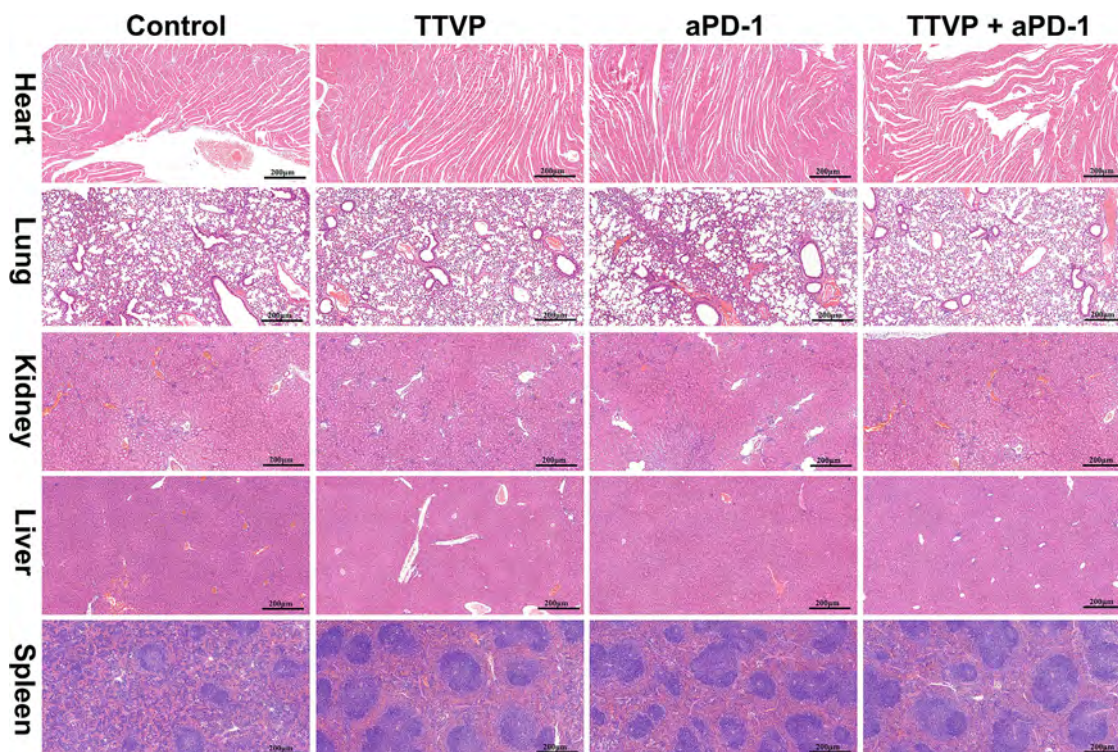


Fig. 10. Micrographs of H&E-stained tissue sections of major organs after different treatment.

cators of immune effect. $\text{TNF-}\alpha$ and IL-12 are the key regulators of the immune response and are highly correlated with antitumor immunity, and their high-level expression is an important indicator for successfully inducing antitumor immune responses [59]. The subsequent antitumor studies using mouse melanoma models showed that the application of TTVP significantly inhibited the growth of melanoma. Moreover, the combined application of TTVP and aPD-1 exhibited a significantly stronger inhibitory effect on tumors than each single treatment, showing an obvious synergistic antitumor effect (Fig. 8). Antitumor cytotoxic T cells are usually CD4^+ or CD8^+ , the two surface molecular markers are essential for immune recognition and killing tumor cells [62]. The proportion of CD4^+ and CD8^+ T cells infiltrating into the tumor tissues is an important indicator of the effect of immunotherapy [62]. The higher the proportion, the better the therapeutic effect and the better the prognosis [63]. Our data suggested that TTVP or/and aPD-1 may induce apoptosis of a large number of tumor cells through promoting CD4^+ and CD8^+ T cells infiltration in tumor tissues (Fig. 9). A recent study has shown that the antitumor activity of aPD-1 depends on DCs expressing IL-12, suggesting that DCs play a key role in tumor immunotherapy [52]. In this study, the application of TTVP and aPD-1 was also observed significantly promoting the expression of IL-12 (Fig. 7), which might be part of the mechanism for the synergistic antitumor effect. Our data indicates that the combination of aPD-1 and DCs-targeted vaccines can significantly enhance the antitumor effect, which provides a new idea for improving the efficacy of immune checkpoint blocking therapy. Since skin tissue is rich in DCs, the combination of DCs-targeted TTVP and immune checkpoint blockers could be an effective strategy for tumor treatment. In addition, our data also shows that the application of TTVP and aPD-1 has good biosafety (Fig. 10).

So far, there are few research reports on TCI used to prevent and treat tumors. Recently, Ye and colleagues reported a TCI system based on microneedles, which can significantly improve the anti-melanoma effect when combined with near-infrared light irradiation [64]. Although microneedles are widely used in transder-

mal drug delivery studies and have been proven to be effective, our Eths-based TCI system has a noninvasive advantage compared to it. To our knowledge, we were the first to report the potential of Eths-based TCI serving in antitumor field [13]. Here, we demonstrated that combination therapy with Eths-based TCI and aPD-1 can produce significant synergistic antitumor effect. Our data also suggested that aPD-1 has prophylactic activities on inhibiting tumor growth and can be an effective adjuvant for antitumor immune, which is worthy of further investigation in the future. For antitumor vaccines, the general view is that the effect of multiple antigens or epitopes is better than that of a single antigen or epitope [65,66]. It should be meaningful to incorporate hybrid antigens into the TTVP system, which may lead to a more ideal antitumor effect.

While the combination of TTVP and aPD-1 shows an excellent antitumor effect, there are some limitations in this study. The significantly increased infiltration of CD4^+ and CD8^+ T cells in tumor tissues after the treatments with TTVP or/and aPD-1 is meaningful for understanding the mechanisms of tumor inhibition, but it would be better if the frequencies of TRP2-specific CD8^+ T cells and basic T cells with reduced exhaustion phenotypes have been investigated. Comparing these data among the groups would provide more clues for understanding the mechanism of synergistic antitumor effect between TTVP and aPD-1. In addition, assessing the phenotype of DCs in lymph nodes following the treatments could better confirm the ability of the vaccines to induce the maturation of DCs in vivo. More comprehensive investigation on phenotypic changes of DCs and T cells in lymphoid organs and tumor microenvironment is required in future studies to understand the detailed mechanism of the antitumor effects of TTVP and aPD-1.

5. Conclusion

In this work, a TTV delivery system was developed by electro-spraying microspheres containing Eth-PEI^{man} onto the electrospun SF-PVA nanofibrous patch. The composite patches showed good

performance of transcutaneous drug delivery. The application of the TTVP loaded with TRP2@Eth-PEI^{man}@CpGs significantly inhibited the growth of melanoma. Furthermore, the combined treatment with TTVP and aPD-1 produced a synergistic antitumor effect, which may be related to the increased infiltration of CD4⁺ and CD8⁺ T cells induced by the treatments. Considering its effectiveness, safety, and easy to use, the combination of TTVP and immune checkpoint blockers could be a promising strategy for tumor prevention and treatment.

Declaration of Competing Interest

There are no conflicts of interest to declare.

Acknowledgements

This research was supported by Science & Technology Commission of Shanghai Municipality (18490740400, 20DZ2254900) and the National Key Research & Development Program of China (2018YFC1706200).

Supplementary materials

Supplementary material associated with this article can be found, in the online version, at doi:10.1016/j.actbio.2021.11.033.

References

- [1] Ralph M Steinman, Decisions about dendritic cells: past, present, and future, *Annu. Rev. Immunol.* 30 (2012) 1–22.
- [2] T Xue, P Liu, Y Zhou, K Liu, L Yang, R.L. Moritz, W. Yan, L.X. Xu, Interleukin-6 induced "acute" phenotypic microenvironment promotes Th1 anti-tumor immunity in cryo-thermal therapy revealed by shotgun and parallel reaction monitoring proteomics, *Theranostics* 6 (06) (2016) 773–794.
- [3] J.A. Mikszta, J.B. Alarcon, J.M. Brittingham, D.E. Sutter, R.J. Pettis, N.G. Harvey, Improved genetic immunization via micromechanical disruption of skin-barrier function and targeted epidermal delivery, *Nat. Med.* 8 (4) (2002) 415–419.
- [4] S.A. Hammond, M. Guebre-Xabier, J. Yu, G.M. Glenn, Transcutaneous immunization: an emerging route of immunization and potent immunostimulation strategy, *Crit. Rev. Ther. Drug Carrier Syst.* 18 (5) (2001) 503–525.
- [5] B. Combadiere, C. Liard, Review of transcutaneous and intradermal vaccination, *Hum. Vaccines* 7 (8) (2011) 811–827.
- [6] Z Chen, Y Lv, J Qi, Q Zhu, Y Lu, W. Wu, Overcoming or circumventing the stratum corneum barrier for efficient transcutaneous immunization, *Drug Discov. Today* 23 (1) (2018) 181–186.
- [7] C.C. Mbah, P.F. Builders, A.A. Attama, Nanovesicular carriers as alternative drug delivery systems: ethosomes in focus, *Expert Opin. Drug Deliv.* 11 (1) (2014) 45–59.
- [8] S.A. Iizhar, I.A. Syed, R. Satar, S.A. Ansari, In vitro assessment of pharmaceutical potential of ethosomes entrapped with terbinafine hydrochloride, *J. Adv. Res.* 7 (2016) 453–461.
- [9] Y Zhang, Q Xia, Y Li, Z He, Z Li, T Guo, Z Wu, N. Feng, CD44 Assists the topical anti-psoriasis efficacy of curcumin-loaded hyaluronan-modified ethosomes: a new strategy for clustering drug in inflammatory skin, *Theranostics* 9 (1) (2019) 48–64.
- [10] Y Zhang, N Zhang, H Song, H Li, J Wen, X Tan, W. Zheng, Design, characterization and comparison of transdermal delivery of colchicine via borneol-chemically-modified and borneol-physically-modified ethosome, *Drug Deliv.* 26 (1) (2019) 70–77.
- [11] S Meng, Z Chen, L Yang, W Zhang, D Liu, J Guo, Y Guan, J. Li, Enhanced transdermal bioavailability of testosterone propionate via surfactant-modified ethosomes, *Int. J. Nanomed.* 8 (2013) 3051–3060.
- [12] L Ma, X Wang, J Wu, D Zhang, L Zhang, X Song, H Hong, C He, X Mo, S Wu, G Kai, H. Wang, Polyethylenimine and sodium cholate-modified ethosomes complex as multidrug carrier for the treatment of melanoma through transdermal delivery, *Nanomedicine (Lond)* 14 (18) (2019) 2395–2408.
- [13] X. Yang, X. Wang, H. Hong, G. Elfawal, S. Lin, J. Wu, Y. Jiang, C. He, X. Mo, G. Kai, H. Wang, Galactosylated chitosan-modified ethosomes combined with silk fibroin nanofibers is useful in transcutaneous immunization, *J. Control. Release* 327 (2020) 88–99.
- [14] W.W. Unger, Y. van Kooyk, Dressed for success' C-type lectin receptors for the delivery of glyco-vaccines to dendritic cells, *Curr. Opin. Immunol.* 23 (2011) 131–137.
- [15] Y. Hattori, S. Kawakami, S. Suzuki, F. Yamashita, M. Hashida, Enhancement of immune responses by DNA vaccination through targeted gene delivery using mannoseylated cationic liposome formulations following intravenous administration in mice, *Biochem. Biophys. Res. Commun.* 317 (4) (2004) 992–999.
- [16] H. Gao, C. Gonçalves, T. Gallego, M. François-Heude, V. Malard, V. Mateo, F. Lemoine, V. Cendret, F. Djedaini-Pilard, V. Moreau, C. Pichon, P. Miodoux, Comparative binding and uptake of liposomes decorated with mannose oligosaccharides by cells expressing the mannose receptor or dc-sign, *Carbohydr. Res.* 487 (2020) 107877.
- [17] M. Cella, D. Scheidegger, K. Palmer-Lehmann, P. Lane, A. Lanzavecchia, G. Alber, Ligation of CD40 on dendritic cells triggers production of high levels of interleukin-12 and enhances T cell stimulatory capacity: T-T help via APC activation, *J. Exp. Med.* 184 (2) (1996) 747–752.
- [18] Q. Han, X. Wang, X. Jia, S. Cai, W. Liang, Y. Qin, R. Yang, C. Wang, CPG loaded MoS₂ nanosheets as multifunctional agents for photothermal enhanced cancer immunotherapy, *Nanoscale* 9 (18) (2017) 5927–5934.
- [19] J. Scheiermann, D.M. Klinman, Clinical evaluation of CPG oligonucleotides as adjuvants for vaccines targeting infectious diseases and cancer, *Vaccine* 32 (48) (2014) 6377–6389.
- [20] H. Zhang, W. Chen, K. Gong, J. Chen, Nanoscale zeolitic imidazolate framework-8 as efficient vehicles for enhanced delivery of CPG oligodeoxynucleotides, *ACS Appl. Mater. Interfaces* 9 (37) (2017) 31519–31525.
- [21] C. Wang, W. Sun, G. Wright, A.Z. Wang, Z. Gu, Inflammation-triggered cancer immunotherapy by programmed delivery of CPG and anti-PD1 antibody, *Adv. Mater.* 28 (40) (2017) 8912–8920.
- [22] A.M. Krieg, Therapeutic potential of toll-like receptor 9 activation, *Nat. Rev. Drug Discovery* 5 (6) (2006) 471–484.
- [23] I. Caminschi, S. Meuter, W.R. Heath, DEC-205 is a cell surface receptor for CPG oligonucleotides, *Proc. Natl Acad. Sci.* 109 (40) (2012) 16270–16275.
- [24] H. Zhang, X.D. Gao, Nanodelivery systems for enhancing the immunostimulatory effect of cpg oligodeoxynucleotides, *Mater. Sci. Eng. C-Mater. Biol. Appl.* 70 (2017) 935–946.
- [25] Y. Xu, Y. Zhu, X. Li, H. Morita, N. Hanagata, Investigation of dendritic mesoporous silica nanoparticles for cytosine-phosphate-guanosine oligodeoxynucleotide delivery, *Mater. Express* 6 (2) (2016) 116–126.
- [26] T. Park, J. Jeong, S. Kim, Current status of polymeric gene delivery systems, *Adv. Drug. Deliv. Rev.* 58 (4) (2006) 467–486.
- [27] A.P. Pandey, K.K. Sawant, Polyethylenimine: a versatile, multifunctional non-viral vector for nucleic acid delivery, *Mater. Sci. Eng. C-Mater. Biol. Appl.* 68 (2016) 904–918.
- [28] Y. Wen, S. Pan, X. Luo, X. Zhang, W. Zhang, M. Feng, A biodegradable low molecular weight polyethylenimine derivative as low toxicity and efficient gene vector, *Bioconj. Chem.* 20 (2) (2009) 322–332.
- [29] T. Cheng, J. Miao, D. Kai, H. Zhang, Polyethylenimine-mediated CPG oligodeoxynucleotide delivery stimulates bifurcated cytokine induction, *ACS Biomater. Sci. Eng.* 4 (3) (2018) 1013–1018.
- [30] Y. Hu, B.-H. Xu, J.-J. Xu, D. Shou, J.-Q. Gao, Synthesis of mannoseylated polyethylenimine and its potential application as cell-targeting non-viral vector for gene therapy, *Polymers* 6 (10) (2014) 2573–2587.
- [31] Y. Hu, B. Xu, Q. Ji, D. Shou, X. Sun, J. Xu, J. Gao, W. Liang, A mannoseylated cell-penetrating peptide-graft-polyethylenimine as a gene delivery vector, *Biomaterials* 35 (2014) 4236–4246.
- [32] Z. Pan, X. Kang, Y. Zeng, A mannoseylated pei-cpp hybrid for trail gene targeting delivery for colorectal cancer therapy, *Polym. Chem.* 8 (2017) 5275–5285.
- [33] Benzoyl peroxide microsphere formulations: what is the science supporting microsphere vehicle technology and clinical use? *J. Clin. Aesthetic Dermatol.* 2 (2009) 46–54.
- [34] F. Wang, L. Feng, G. Li, Z. Zhai, H. Ma, B. Deng, S. Zhang, Fabrication and properties of superhydrophobic waterborne polyurethane composites with micro-rough surface structure using electrostatic spraying, *Polymers* (2009) 11.
- [35] C.P. Barnes, S.A. Sell, E.D. Boland, D.G. Simpson, G.L. Bowlin, Nanofiber technology: designing the next generation of tissue engineering scaffolds, *Adv. Drug. Deliv. Rev.* 59 (2007) 1413–1433.
- [36] X. Yang, L. Fan, L. Ma, Y. Wang, S. Lin, F. Yu, X. Pan, G. Luo, D. Zhang, H. Wang, Green electrospun Manuka honey/silk fibroin fibrous matrices as potential wound dressing, *Mater. Des.* 119 (2017) 76–84.
- [37] P. Chantawong, T. Tanaka, A. Uemura, K. Shimada, A. Higuchi, H. Tajiri, K. Sakura, T. Murakami, Y. Nakazawa, R. Tanaka, Silk fibroin-Pellethane® cardiovascular patches: effect of silk fibroin concentration on vascular remodeling in rat model, *J. Mater. Sci. Mater. Med.* 28 (2017) 191.
- [38] C. Steffi, D. Wang, C.H. Kong, Z. Wang, P.N. Lim, Z. Shi, E. San Thian, W. Wang, Estradiol-loaded poly(ε-caprolactone)/silk fibroin electrospun microfibers decrease osteoclast activity and retain osteoblast function, *ACS Appl. Mater. Interfaces* 10 (2017) 9988–9998.
- [39] J. Luo, H. Zhang, J. Zhu, X. Cui, J. Gao, X. Wang, J. Xiong, 3-D mineralized silk fibroin/polycaprolactone composite scaffold modified with polyglutamate conjugated with BMP-2 peptide for bone tissue engineering, *Colloids Surf. B Biointerfaces* 163 (2018) 369–378.
- [40] S.A. Kheradvar, J. Nourmohammadi, H. Tabesh, B. Bagheri, Starch nanoparticle as a vitamin E-TPGS carrier loaded in silk fibroin-poly(vinyl alcohol)-Aloe vera nanofibrous dressing, *Colloids Surf. B Biointerfaces* 166 (2018) 9–16.
- [41] P. Bhattacharjee, B. Kundu, D. Naskar, T.K. Maiti, D. Bhattacharya, S.C. Kundu, Nanofibrous nonmulberry silk/PVA scaffold for osteoinduction and osseointegration, *Biopolymers* 103 (2015) 271–284.
- [42] T. Zhang, J. Gu, X. Liu, D. Wei, H. Zhou, H. Xiao, Z. Zhang, H. Yu, S. Chen, Bactericidal and antifouling electrospun PVA nanofibers modified with a quaternary ammonium salt and zwitterionic sulfopropylbetaine, *Mater. Sci. Eng. C, Mater. Biol. Appl.* 111 (2020) 110855.
- [43] S.L. Topalian, F.S. Hodi, J.R. Brahmer, S.N. Gettinger, D.C. Smith, D.F. McDermott, J.D. Powderly, R.D. Carvajal, J.A. Sosman, M.B. Atkins, P.D. Leming, D.R. Spiegel,

- S.J. Antonia, L. Horn, C.G. Drake, D.M. Pardoll, L. Chen, W.H. Sharfman, R.A. Anders, J.M. Taube, T.L. McMiller, H. Xu, A.J. Korman, M. Jure-Kunkel, S. Agrawal, D. McDonald, G.D. Kollia, A. Gupta, J.M. Wigginton, M. Sznol, Safety, activity, and immune correlates of anti-PD-1 antibody in cancer, *N. Engl. J. Med.* 366 (2012) 2443–2454.
- [44] S. Yao, Y. Zhu, L. Chen, Advances in targeting cell surface signalling molecules for immune modulation. *Nature reviews, Drug Discov.* 12 (2013) 130–146.
- [45] A. Forschner, F. Battke, D. Hadaschik, M. Schulze, S. Weißgraeber, C.T. Han, M. Kopp, M. Frick, B. Klumpp, N. Tietze, T. Amaral, P. Martus, T. Sinnberg, T. Eigentler, U. Keim, C. Garbe, D. Döcker, S. Biskup, Tumor mutation burden and circulating tumor DNA in combined CTLA-4 and PD-1 antibody therapy in metastatic melanoma - results of a prospective biomarker study, *J. Immunother. Cancer* 7 (2019) 180.
- [46] S. Aspeslagh, R.M. Chabanon, S. Champiat, S. Postel-Vinay, Understanding genetic determinants of resistance to immune checkpoint blockers, *Semin. Cancer Biol.* 65 (2020) 123–139.
- [47] J. Fu, D.B. Kanne, M. Leong, L.H. Glickman, S.M. McWhirter, E. Lemmens, K. Mechette, J.J. Leong, P. Lauer, W. Liu, K.E. Sivick, Q. Zeng, K.C. Soares, L. Zheng, D.A. Portnoy, J.J. Woodward, D.M. Pardoll, T.W. Dubensky Jr., Y. Kim, Sting agonist formulated cancer vaccines can cure established tumors resistant to PD-1 blockade, *Sci. Transl. Med.* 7 (2015) 283–252.
- [48] M. Segovia, S. Russo, M. Jeldres, Y.D. Mahmoud, V. Perez, M. Duhalde, P. Charney, M. Rousset, S. Victoria, F. Veigas, C. Louvet, B. Vanhove, R.A. Floto, I. Aneagon, M.C. Cuturi, M.R. Girotti, G.A. Rabinovich, M. Hill, Targeting TMEM176B enhances antitumor immunity and augments the efficacy of immune checkpoint blockers by unleashing inflammasome activation, *Cancer Cell* 35 (2019) 767–781.
- [49] S. Nakao, Y. Arai, M. Tasaki, M. Yamashita, R. Murakami, T. Kawase, N. Amino, M. Nakatake, H. Kurosaki, M. Mori, M. Takeuchi, T. Nakamura, Intratumoral expression of IL-7 and IL-12 using an oncolytic virus increases systemic sensitivity to immune checkpoint blockade, *Sci. Transl. Med.* 12 (2019).
- [50] M. Wang, Y. Liu, Y. Cheng, Y. Wei, X. Wei, Immune checkpoint blockade and its combination therapy with small-molecule inhibitors for cancer treatment, *Biochimica et Biophysica Acta. Rev. Cancer* 1871 (2019) 199–224.
- [51] H. Ruan, L. Bu, Q. Hu, H. Cheng, W. Lu, Z. Gu, Strategies of combination drug delivery for immune checkpoint blockades, *Adv. Healthc. Mater.* 8 (2019) 180–199.
- [52] C.S. Garriss, S.P. Arlauckas, R.H. Kohler, M.P. Trefny, S. Garren, C. Piot, C. Engblom, C. Pfirschke, M. Siwicki, J. Gungabeesoon, G.J. Freeman, S.E. Warren, S. Ong, E. Browning, C.G. Twitty, R.H. Pierce, M.H. Le, A.P. Algazi, A.I. Daud, S.I. Pai, A. Zippelius, R. Weissleder, M.J. Pittet, Successful anti-PD-1 cancer immunotherapy requires T cell-dendritic cell crosstalk involving the cytokines IFN- γ and IL-12, *Immunity* 49 (2019) 1148–1161.
- [53] Y. Jeong, G.B. Kim, Y. Ji, G.J. Kwak, G.H. Nam, Y. Hong, S. Kim, J. An, S.H. Kim, Y. Yang, H.S. Chung, I.S. Kim, Dendritic cell activation by an E. coli-derived monophosphoryl lipid A enhances the efficacy of PD-1 blockade, *Cancer Lett.* 472 (2020) 19–28.
- [54] Y. Xia, G. Tang, C. Wang, J. Zhong, Y. Chen, L. Hua, Y. Li, H. Liu, B. Zhu, Functionalized selenium nanoparticles for targeted siRNA delivery silence Derlin1 and promote antitumor efficacy against cervical cancer, *Drug Deliv.* 27 (2020) 15–25.
- [55] J. He, S. Duan, X. Yu, Z. Qian, S. Zhou, Z. Zhang, X. Huang, Y. Huang, J. Su, C. Lai, J. Meng, N. Zhou, X. Lu, Y. Zhao, Folate-modified chitosan nanoparticles containing the IP-10 gene enhance melanoma-specific cytotoxic CD8(+)/CD28(+) T lymphocyte responses, *Theranostics* 6 (2016) 752–761.
- [56] M. Zhu, X. Ding, R. Zhao, X. Liu, H. Shen, C. Cai, M. Ferrari, H.Y. Wang, R.F. Wang, Co-delivery of tumor antigen and dual toll-like receptor ligands into dendritic cell by silicon microparticle enables efficient immunotherapy against melanoma, *J. Control. Release* 272 (2018) 72–82.
- [57] C. Lai, S. Duan, F. Ye, X. Hou, X. Li, J. Zhao, X. Yu, Z. Hu, Z. Tang, F. Mo, X. Yang, X. Lu, The enhanced antitumor-specific immune response with mannose- and CPG-ODN-coated liposomes delivering Trp2 peptide, *Theranostics* 8 (2018) 1723–1739.
- [58] E.A. Vasievich, S. Ramishetti, Y. Zhang, L. Huang, Trp2 peptide vaccine adjuvanted with (R)-DOTAP inhibits tumor growth in an advanced melanoma model, *Mol. Pharm.* 9 (2012) 261–268.
- [59] Q. Zeng, H. Jiang, T. Wang, Z. Zhang, T. Gong, X. Sun, Cationic micelle delivery of Trp2 peptide for efficient lymphatic draining and enhanced cytotoxic T-lymphocyte responses, *J. Control. Release* 200 (2015) 1–12.
- [60] R. Goyal, L.K. Macri, H.M. Kaplan, J. Kohn, Nanoparticles and nanofibers for topical drug delivery, *J. Control. Release* 240 (2016) 77–92.
- [61] M.B. Rask, M.M. Knopp, N.E. Olesen, R. Holm, T. Rades, Influence of PVP/VA copolymer composition on drug-polymer solubility, *Eur. J. Pharm. Sci.* 85 (2012) 10–17.
- [62] J.M. Silva, E. Zupancic, G. Vandermeulen, V.G. Oliveira, A. Salgado, M. Videira, M. Gaspar, L. Graca, V. Pr at, H.F. Florindo, In vivo delivery of peptides and Toll-like receptor ligands by mannose-functionalized polymeric nanoparticles induces prophylactic and therapeutic anti-tumor immune responses in a melanoma model, *J. Control. Release* 198 (2015) 91–103.
- [63] M. Huo, Y. Zhao, A.B. Satterlee, Y. Wang, Y. Xu, L. Huang, Tumor-targeted delivery of sunitinib base enhances vaccine therapy for advanced melanoma by remodeling the tumor microenvironment, *J. Control. Release* 245 (2017) 81–94.
- [64] Y. Ye, C. Wang, X. Zhang, Q. Hu, Y. Zhang, Q. Liu, D. Wen, J. Milligan, A. Bellotti, L. Huang, G. Dotti, Z. Gu, A melanin-mediated cancer immunotherapy patch, *Sci. Immunol.* 2 (2017) eaan5692.
- [65] I. Algarra, A. Garcia-Lora, T. Cabrera, F. Ruiz-Cabello, F. Garrido, The selection of tumor variants with altered expression of classical and nonclassical MHC class I molecules: implications for tumor immune escape, *Cancer Immunol. Immunother.* 53 (2004) 904–910.
- [66] S. Walter, T. Weinschenk, Muropeptide immune response to cancer vaccine IMA901 after single-dose cyclophosphamide associates with longer patient survival, *Nat. Med.* 18 (2012) 1254–1261.